Article:
Graves, KA, Higgins, LJR orcid.org/0000-0001-5375-7902, Nahil, MA et al. (2 more authors) (2022) Structural comparison of multi-walled carbon nanotubes produced from polypropylene and polystyrene waste plastics. Journal of Analytical and Applied Pyrolysis, 161. 105396. ISSN 0165-2370

https://doi.org/10.1016/j.jaap.2021.105396

Structural comparison of multi-walled carbon nanotubes produced from polypropylene and polystyrene waste plastics

Katherine Graves, Luke J.R. Higgins, Mohamad A. Nahil, Bhoopesh Mishra, Paul T. Williams*

School of Chemical and Process Engineering, University of Leeds, Leeds LS2 9JT, UK
(*Corresponding author; Email; p.t.williams@leeds.ac.uk; Tel; #44 1133432504)

ABSTRACT

Polypropylene and polystyrene were processed in a pyrolysis/catalytic reactor with a Ni-Fe/Al_2O_3 catalyst to produce carbon nanotubes (CNTs). A high yield of catalyst carbon deposits were produced; 33.5 g 100 g^{-1} polypropylene and 29.5 g 100g^{-1} polystyrene and consisted of multi-walled carbon nanotubes (MWCNTs). X-ray diffraction (XRD) of the Ni-Fe/Al_2O_3 catalyst suggested the active metal was a Ni-Fe alloy which was confirmed using X-ray absorption near edge structure (XANES); extended X-ray absorption fine structure (EXAFS) analysis showed that the alloy was primarily $FeNi_2$. Electron microscopy showed that the MWCNTs were entangled, several μm in length and ~50 nm in diameter comprising ~30 graphene layers. Optical Raman spectroscopy confirmed the carbons to be of high purity and crystallinity with polypropylene showing a higher degree of graphitisation and fewer defects compared to those produced from polystyrene. X-ray Raman scattering spectroscopy of the MWCNTS confirmed their graphitic carbon composition, but demonstrated poor alignment. Commercially produced MWCNTs showed a high degree of graphitisation, with less metal impurities and were of long length (several μm), straighter, smaller diameter (~10 nm) and with fewer number of graphene layers (~12) in the CNT wall compared with the plastic derived MWCNTs.

Keywords: Carbon nanotubes; Catalyst; Plastics; Pyrolysis; Waste

1. INTRODUCTION

Multi walled carbon nanotubes (MWCNTs) have unique, physical and electrical properties with wide application in a number of different industrial sectors.[1-5] , Commercially, MWCNTs are typically produced from fossil-derived carbon precursors such as acetylene, benzene, xylene or methane by chemical vapour deposition (CVD).[5] The CVD process involves passing the gaseous precursor over a catalyst containing metal nano-particles held at a temperature between 600 °C and 1200 °C and where the carbon nanotubes are formed. Many studies have shown that a variety of carbonaceous wastes can be used as an alternative feedstock for MWCNTs; these include waste tyres,[6] bamboo charcoal,[7] rice straw,[8] wood sawdust,[9] lignin [10] and cellulose.[11]

One of the most common waste materials with a high carbon and volatile content suitable for the production of MWCNTs are waste plastics. Europe produces an estimated 29 Mt of plastic waste each year[12] and represents an enormous waste management issue and environmental problem.[13,14] Process routes for waste plastics in Europe include, waste landfill, energy recovery through waste incineration and recycling. However, recycling of waste plastics currently represents only ~32.5% of European waste plastic arisings.[12] The vast majority (~99%) of recycling of waste plastics is *via* mechanical recycling to produce low grade products.[15] However, there is interest in producing higher value products from waste plastics and there is a growing body of research into the production of MWCNTs from waste plastics.[16, 17] The process of producing MWCNTs from waste plastics commonly involves an adaption of the CVD process for the commercial production of MWCNTs from pure hydrocarbon gases. The process involves the thermal degradation of the waste plastics by pyrolysis to produce hydrocarbon gases which are then passed to a chemical vapour deposition (catalyst) reactor for the production of MWCNTs. [18-22] During pyrolysis, the plastic is converted to a pyrolysis gas containing a suite of hydrocarbons that pass over a catalyst in the CVD reactor containing metal nano-particles that seed CNT growth. The main plastics found in municipal solid waste, as post-consumer household plastic waste are, high-density polyethylene (HDPE), low density polyethylene (LDPE), polypropylene (PP), polystyrene (PS), polyvinylchloride (PVC) and polyethylene terephthalate (PET).[23] The different chemical composition and structures of the polymers will produce different thermal degradation products during

pyrolysis [24] and will therefore influence the production of MWCNTs during CVD. For example, the shape and structure of product CNTs is influenced by plastic type; Chung et al. [25] investigated the production of CNTs from polypropylene and polystyrene and reported differences in the morphology of the product CNTs due to the differences in the chemical structure of the polymers and the consequent derived aromatic or alkene CNT precursors. Cai et al.,[26] reported that polypropylene and polyethylene produced more graphitic carbon nanotubes compared to polystyrene, which also contained more amorphous carbon. The physical morphology of the product carbons was also influenced by the plastic type.

The type of catalyst used to produce carbon nanotubes from waste plastics are most commonly based around those currently used for commercial production and include Fe, Co and Ni based catalysts.[27,28] . In our previous work [29] we showed that Fe-alumina and Ni-alumina catalysts produced higher yields of carbon nanotubes compared to Co- and Cu-alumina catalysts. This was attributed to the optimum (intermediate) metal-support interaction of Ni and Fe which enabled CNT growth, due to vapour-solid-solid growth affecting the decomposition of carbon-containing precursors, diffusion of carbon atoms and precipitation at the metal-support interface. But for Co-alumina the metal-support interaction was too strong, preventing the formation of nano-metal particles that could easily detach from the support and participate in CNT growth. However, interaction between Cu and the support was weak, producing sintering of the metal and formation of large particles and consequently low CNT production.[29] Direct comparison of different metals for CNT production was also carried out by Liu et al.[30] and showed that Fe was superior to Ni- and Co-based catalysts for the production of CNTs from methane, due to the higher solubility of carbon in the Fe particles. However, Lee et al.[31] reported that a Ni catalyst produced a higher CNT yield compared to an Fe catalyst using acetylene as the feedstock. Work by Yao and Wang [25] using waste plastic (polypropylene) as the feedstock found that CNT yield was highest for a Fe-catalyst compared to a Ni-catalyst, but interestingly, a Ni-Fe catalyst was superior to both Fe and Ni catalysts. This was attributed to the enhanced Ni-Fe metal reducibility and synergistic effects between Fe and Ni bimetallic species and their interaction with the support material. Ratkovic et al. [32] also reported a markedly higher yield of CNTs for a Ni-Fe-alumina catalyst compared to Fe-alumina for the production of CNTs from ethylene. It

was suggested that the addition of the second metal enhanced metal-support interaction. Kutteri et al.[33] reported that bimetallic-SiO_2 catalysts (Ni, Fe, Co) produced smaller crystallite sizes and possessed higher stability for CNTs production from methane compared with Ni-SiO_2 and Fe-SiO_2 catalysts. Further investigation into the use of bi-metallic Ni-Fe-alumina catalysts for CNT production investigated the ratio of Ni:Fe molar ratio on the yield and characteristics of the product CNTs using waste plastics as the feedstock.[34] It was reported that higher loading of Fe in the Ni-Fe bimetallic catalyst produced a higher yield of CNTs, but higher Ni loading produced CNTs with narrower diameters and more uniform distribution. It was suggested that the presence of Ni improved the thermal stability of the product CNTs and they exhibited less defects and a higher degree of graphitisation. The nature of the support material has also been shown to be an important factor in determining the yield and the characteristics of the product CNTs from the Ni-Fe bimetallic catalysts, affecting the shape, purity and graphitisation of the CNTs.[35]

The research into the use of bimetallic Ni-Fe catalysts for MWCNTs production is progressing, but there is a further need to investigate the characteristics of the CNTs produced from the pyrolysis/catalysis of different types of waste plastics. In particular, characterisation of CNTs produced from waste plastics using advanced analytical techniques enables a better understanding of the influence that polymer structure has on the shape, purity and degree of graphitisation of the product CNTs. The most common analytical techniques used to characterise MWCNTs produced from waste plastics include: temperature programmed oxidation (TPO), Raman spectroscopy and transmission electron microscopy (TEM). Such techniques enable comparison of the product MWCNTs from waste plastics with those produced commercially using the CVD process from pure hydrocarbon feedstocks. TPO analysis uses thermogravimetric analysis with air as the carrier gas and is used to differentiate between the different types of carbon deposits formed on the catalyst in the CVD reactor, such as amorphous carbon, filamentous solid carbon nano-fibres and MWCNTs.[36] The process is based on the different oxidation temperatures of the different types of carbon. Raman spectroscopy is used to characterise the catalyst carbon deposits and indicate the presence and quality of any MWCNTs in terms of crystallinity.[37] In a Raman spectrum, there are three peaks (bands), characteristic of CNTs; the *D* band at a wavelength of ~1350 cm^{-1}, the *G* band at

~1580 cm^{-1} and the *G′* band at ~1350 cm^{-1}. In addition, the ratio of the different bands indicating the purity of the MWCNTs, the degree of graphitisation and the presence of defects. Electron microscopy is a valuable technique for imaging samples and identifying the presence of MWCNTs. Scanning electron microscopy (SEM) is routinely used to determine whether filamentous type carbons are present within a sample;[37] however, there is no ability to differentiate between CNTs and solid carbon nano-fibres, or to determine how many walls are present in the MWCNTs. Therefore, TEM is used to identify whether any filamentous carbons are hollow (CNTs) or solid (carbon nano-fibres). Furthermore, the number of walls can be counted as they are visible on a TEM image, as length scales of <5 nm can be reached. Using a combination or all of these techniques means that the presence of MWCNTs can be identified with confidence and their quality and dimensions can be assessed with a view to optimising their properties to particular end-use applications.

Spectroscopy of produced CNTs is commonly used to monitor the development of local structure during formation. In particular, optical Raman, electron energy loss (EELS) and X-ray photoelectron (XPS) spectroscopy have been used to monitor the development of heteroatom (e.g. O, N) functionality within CNTs, which can have a significant effect on their final application.[38] Each of these techniques is limited to a few nanometres of penetration in the produced CNT, which can result in errors due to spectral distortion. X-ray Raman scattering (XRS) spectroscopy can further enhance the characterisation and assess the quality of MWCNTs. XRS spectroscopy is a 'photon-in-photon-out' X-ray spectroscopy technique as opposed to 'photon-in electron out' techniques such as X-ray photoelectric spectroscopy (XPS). XRS spectroscopy is able to probe the bulk chemistry of low-Z elements (e.g. C, N, O) using hard X-ray (i.e. 10 KeV) photons.[39,40] Similarly to EELS or XPS, XRS spectroscopy can be used as a bulk probe to investigate sp^2 and sp^3 carbon hybridization in CNTs, as performed in other studies.[41] In addition, a more detailed bulk structural comparison can be made with MWCNTs produced commercially from pure hydrocarbon feedstocks.

In this paper, CNTs were produced from two structurally different plastics, polypropylene and polystyrene, using a two-stage pyrolysis/catalysis process similar to the pyrolysis/CVD process with a Ni-Fe/Al_2O_3 catalyst. The MWCNTs obtained from each plastic were fully characterised using TPO, Raman (optical) spectroscopy, SEM, TEM and

XRS. Here, XRS spectroscopy has been used to determine whether any differences in bulk carbon chemistry exist between MWCNTs produced from an aliphatic structured plastic polymer (polypropylene) compared with MWCNTs produced from an aromatic structured plastic polymer (polystyrene). In addition, the different characterisation techniques were applied to commercially obtained MWCNTs to compare with the characteristics of the MWCNTs obtained from the waste plastics.

2. EXPERIMENTAL

2.1. Plastic samples

The plastic materials used were 'real-world' recycled plastic wastes, polypropylene representing an aliphatic structured polymer and polystyrene representing an aromatic structured polymer. The waste plastics were obtained from Regain Polymers Ltd., Castleford, UK. Proximate and ultimate analyses of the polypropylene and polystyrene are shown in Table 1. Both plastics have similar properties, with almost 100 wt.% volatile content. Ultimate analysis showed that polystyrene contained more carbon and less hydrogen compared with polypropylene, commensurate with their chemistry (polypropylene, $(C_3H_6)_n$) and polystyrene, $(C_8H_8)_n$). The presence of ash, sulphur and oxygen in the plastic samples which may be due to impurities introduced during the recycling process such as polyethylene terephthalate. In addition, commercial post-consumer plastics may contain several different additives, such as anti-oxidants, UV absorbers, inorganic fillers etc, used to improve the properties of the plastic in relation to their end-use application. The carbon contents of the pure polypropylene and polystyrene are 85.6 wt.% and 92.2 wt.%, respectively,[16] therefore the waste plastic samples used in this study contain some contamination from other waste plastics or additives.

2.2. Commercial carbon nanotubes.

The commercial multi-walled carbon nanotubes were produced by CVD with subsequent demineralisation using hydrochloric acid and were obtained from Sigma-Aldrich Ltd., UK. The commercial MWCNTs were >98% carbon composition, of length range 2.5 - 20 μm

and average length 10 μm as determined by TEM. The diameter of the MWCNTs was between 6 nm - 13 nm with an average diameter 12 nm and wall thickness of between 7 - 13 graphene layers as determined by high resolution TEM imaging. The BET surface area was ~220 m^2 g^{-1}. The commercially obtained MWCNTs are referred to as 'com-MWCNT' in this paper.

2.3. Catalyst preparation and characterisation

The Ni-Fe catalyst on an alumina support (Ni-Fe/Al_2O_3) was produced using a wet impregnation method. Nickel nitrate and iron nitrate were dissolved in distilled water and combined with powdered alumina. The mass of powdered alumina and $Ni(NO_3)_2$ and $Fe(NO_3)_2$ were calculated to produce a catalyst with 5 wt.% Ni and 5 wt.% Fe content to produce a 10wt.% Ni-Fe/Al_2O_3 catalyst. The $Ni(NO_3)_2$, $Fe(NO_3)_2$ and alumina solution was slowly heated to ~90 °C to evaporate most of the water and form a slurry, which was dried at 105 °C for 12 hours prior to calcination. Calcination took place in an air atmosphere heated from room temperature to 750 °C at a heating rate of 20 °C min^{-1} with a hold time of 3 hours at a temperature of 750 °C. The catalysts were crushed and sieved to ensure a particle size distribution between 50 μm and 210 μm. The final step was reduction of the catalyst in a hydrogen atmosphere (5 vol.% H_2 and 95 vol.% N_2). The reduction conditions were a heating rate of 20 °C min^{-1} from room temperature to a final temperature of 800 °C with a hold time of 3 hours. The prepared Ni-Fe/Al_2O_3 catalyst had a BET surface area of 124.4 m^2 g^{-1}, determined using a Quantachrome Nova-2020 instrument *via* N_2 adsorption/desorption isotherms at 77K. The catalyst was also characterised in terms of crystalline properties by powder X-ray diffraction (XRD) with a Bruker D8 powder X-ray diffractometer operated at 40 kV and 40 mA.

The Ni-Fe/Al_2O_3 catalyst was also analysed by X-ray Absorption Fine Structure (XAFS) spectroscopy encompassing X-ray Absorption Near Edge Structure (XANES, measurements taken around the absorption edge energy) and Extended X-ray Absorption Fine Structure (EXAFS, measurements taken approximately 30 eV past absorption edge energy) to determine the catalyst chemistry. XAFS is a synchrotron X-ray technique that uses hard X-rays (~10keV) and yields information about interatomic distances, coordination number and here, was used to determine whether the Ni and Fe

within the catalyst were elemental or a Ni-Fe alloy. Analysis was conducted at the bending magnet beamline 20-BM of the Advanced Photon Source (APS) in the Argonne National Laboratory (USA). IFEFFIT software package including ATHENA and ARTEMIS was used to analyse the EXAFS data using a shell-by-shell fitting approach. The data range used for Fourier Transformation (FT) of the EXAFS data was k = 3.0–10.5Å^{-1}. Fitting range for obtaining best fits was 1.0–5.5Å, using a Hanning window function with dk = 1.

2.4. Pyrolysis/CVD reactor system

A two-stage, fixed bed pyrolysis/CVD reactor system was used to produce CNTs with waste polypropylene and polystyrene as the feedstock. A schematic diagram of the reactor system is shown in Figure 1. The reactor had a total length of 50 cm and 2.5 cm in diameter and was constructed from stainless steel and each stage was separately heated and temperature controlled using two separate electrical furnaces. Pyrolysis of the plastic waste took place in the first stage and the resultant pyrolysis gases/vapours were passed directly to the second stage CVD catalyst reactor where the 10wt.% Ni-Fe/Al_2O_3 catalyst was located. The plastic waste (2.0 g) was held centrally in the pyrolysis reactor in a stainless-steel crucible and the catalyst was located centrally in the CVD reactor as a bed of catalyst (1.0 g) supported on quartz wool. Both reactors were continuously purged with inert N_2 carrier gas. The volatile products exiting the CVD reactor were passed through a condenser system, cooled with water and dry ice to ensure any condensable products were removed from the gas stream. Any remaining gaseous products were collected in a 25 l Tedlar^{TM} gas sample bag for immediate off-line gas analysis.

For each experiment, the CVD catalyst reactor was pre-heated to 800 °C and held at that temperature throughout the experiment. This temperature was chosen as our previous work [18] has shown that CNT synthesis temperatures of 800 °C give the highest yield of carbon deposits on the catalyst in the pyrolysis/CVD process using waste plastics. Once the catalyst temperature had stabilised at 800 °C, the pyrolysis reactor was heated to 600 °C for the pyrolysis of polypropylene or 500 °C in the case of polystyrene pyrolysis, at a heating rate of 20 °C min^{-1} and held for 20 minutes at the maximum temperature. The final pyrolysis temperatures of the two waste plastics were determined from preliminary thermogravimetric analysis (TGA - Mettler Toledo TGA/DSC3+) experiments in an N_2

atmosphere. The peak temperature of the derivative TGA thermogram determined the thermal degradation temperatures of the polypropylene and polystyrene. At the end of the pyrolysis process, the N_2 was allowed to flow through the system for a further 20 minutes to ensure all product gases were purged from the reactor.

2.5. Product characterisation and analysis

2.5.1. Gas analysis

Packed column gas chromatography (GC) was used to analyse the gaseous products collected in the gas sample bag. Permanent gases (H_2, CO, O_2 and N_2) were analysed using a Varian 3380 GC/TCD (thermal conductivity detector) with argon as the carrier gas with a 60-80 mesh HayeSep packed column, 2 m long and 2 mm in diameter. The GC used for CO_2 analysis was a second Varian 3380 GC fitted with a packed molecular sieve column (80-100 mm mesh) and TCD but a different GC temperature programme was used to enable peak separation of co-eluting CO_2 and CO which. Hydrocarbon gases (C_1-C_4) were measured using a third Varian 3380 GC/FID (flame ionisation detector) with nitrogen as the carrier gas and a 2 m long and 2 mm diameter column packed with 80-100 mesh HayeSep. The different gas chromatographs were calibrated with known concentrations of standard gas mixtures and gas yield was determined by calculation, rather than 'by difference'. Calculation was from the known nitrogen purge gas flow rate, the volumetric composition and concentration of each gas coupled with the Ideal Gas Law and known density of each gas. Thereby, the total gas yield was determined from the individual gas mass data.

2.5.2. Characterisation of catalyst carbon deposits

A variety of techniques were used to measure and analyse the carbon deposits on the used 10 wt.% Ni-Fe/Al_2O_3 catalyst from the pyrolysis/CVD processing of the polypropylene and polystyrene. In addition, the commercially obtained MWCNTs (Com-MWCNTs - Sigma-Aldrich Ltd. UK) were also analysed for comparison with the waste derived nano-

carbon materials. The carbon deposit yield was determined by mass balance, i.e. weighing the CVD reactor tube and catalyst before and after the reaction.

Temperature programmed oxidation (TPO) via thermogravimetric analysis (TGA) was conducted to determine the type of carbon deposited on the catalyst, in terms of the amount of amorphous and graphitic carbon. TPO was conducted on a Mettler Toledo TGA/DSC3+ TGA with an air atmosphere, TGA oven heating rate of 15 °C min^{-1}, heating the sample from ambient temperature to a maximum temperature of 800 °C with a hold time of 10 minutes.

The determination of the graphitic quality of the polypropylene and polystyrene derived carbon deposits and com-MWCNTs was investigated using optical Raman spectroscopy, which was conducted on a Renishaw Invia Raman spectrometer. A laser at a wavelength of 540 nm was used to measure Raman shifts between 100 and 3200 cm^{-1}.

High-resolution scanning electron microscopy (HR-SEM) was undertaken using an Hitachi SU8230 field emission gun SEM. Samples for SEM were prepared by sputter coating 5 nm of Ir on the sample using a high-resolution sputter coater(Agar Scientific, UK). Samples for HR-TEM were prepared by dispersion in water onto amorphous holey carbon support films on copper grids (Agar, UK). Samples were mounted onto a double-tilt TEM holder (FEI, UK). HR-TEM imaging was performed using an FEI Titan^3 Themis G2 S/TEM operating at 300 kV.

X-ray Raman scattering (XRS) spectroscopy is a synchrotron X-ray technique that measures non-resonant inelastic scattering, where an incoming monochromatic photon loses energy and changes momentum through an interaction with a core electron in the sample.[39] XRS spectroscopy is an element selective technique that can be used to monitor bonding and functionalities within a sample. Hard X-ray photons are used to study the photo-absorption spectra of low-Z elements without the limitations of soft X-ray measurements, such as low penetration depths and self-absorption effects. Here, XRS spectroscopy was conducted at beamline ID-20 of the European Synchrotron Radiation Facility (ESRF), Fr. At ID-20, an undulator is used to produce incident radiation which is subsequently monochromatised using a cryogenically-cooled Si (311) double-crystal monochromator. The monochromatic beam was focussed to ~10µm×10µm using a Kirkpatrick-Baez mirror system and directed onto the pelletised sample in low-angle scattering geometry. The XRS spectrometer at ID-20 is comprised of 72 spherically bent

Si(660) crystal analysers, however this work only used the 36 analysers that were at low momentum transfer, *q*. The average *q* was 1.81 $Å^{-1}$. Measurements were performed by fixing the energy of the scattered X-rays from the analyser crystals (9690eV) and scanning the monochromator energy (9950 –10*1*00 eV).The core carbon *K*-edge was measured with an overall energy resolution of 0.65eV (taken from FWHM of the elastic peak). Averaging and background subtraction of energy-loss spectra was carried out using the XRS tools software suite.[42] Background subtraction was performed against a Hartree–Fock calculated core atomic carbon *K*-edge profile with a parameterised Pearson VII function background. Background subtracted and normalised XRS spectra from the waste plastic derived and commercial MWCNTs were fitted using Gaussian curves to represent the core electron resonances of relevant carbon functionalities and an exponentially-decaying step function to represent the edge.[43] Spectral fitting used a Gaussian non-linear least-squares fitting LMFIT software [44] based on the full-width half maxima (FWHM) of the selected Gaussian functions. Table 2 shows the different forms of carbon structural groups and corresponding peak energy transition ranges used for the Gaussian fitting. [45-49] Here, we use XRS spectroscopy for the first time to measure carbon chemistry of waste plastic-derived MWCNTs to understand their functionalities and suggest suitable end-use applications.

3. RESULTS AND DISCUSSION

3.1. Product yield from the pyrolysis/CVD processing of polypropylene and polystyrene.

The product yield from the two-stage, pyrolysis/CVD processing of waste polypropylene and polystyrene is shown in Table 3. Also shown are the product gas composition (vol.%). The pyrolysis/CVD process produced a significantly higher gas yield for the processing of polypropylene (36.3 wt.%) compared with polystyrene (15.6 wt%). This may be attributed to the linear aliphatic polymer structure of the polypropylene enabling an easier thermal degradation due to the lower bond dissociation energy of the C —C bond to produce lower molecular weight gaseous products. The polystyrene polymer is based on the stable aromatic benzene ring structure with a higher bond dissociation energy for the C = C

bond, resulting in heavier molecular weight products. The product oil yield shown in Table 3 will contain mainly aliphatic compounds for the polypropylene and aromatic compounds for the polystyrene.[24] In addition, the presence of the CVD catalyst at high temperature (800 °C) serves to further thermally degrade the higher molecular weight compounds, with higher levels of bond scission and hence increased C_1 — C_4 gases. Table 3 also shows the gas composition from the pyrolysis/CVD processing of polypropylene and polystyrene, showing that the main gases produced were C_1 — C_4 hydrocarbons and hydrogen produced from high temperature catalytic degradation of the product gases/vapours produced from the pyrolysis of the plastics. The high concentrations of hydrogen and C_1 — C_4 hydrocarbons in the product gas produce a high calorific value gas that could be used as process fuel for the pyrolysis/CVD process. The lower concentrations of carbon oxide gases (CO and CO_2) are most probably produced from contaminants, such as polyethylene terephthalate plastic in the recycled waste plastics or alternatively from oxygen containing additives used in polymer manufacture. The low char yield would also likely contain some contaminants or additives from the plastics recycling process.

3.2. Catalyst characterisation

The used Ni-Fe/Al_2O_3 catalyst after pyrolysis/CVD processing of polypropylene and polystyrene were analysed by powder X-ray diffraction (XRD) and XAFS. Annotated XRD diffractograms are shown in Figure 2. Also shown in Figure 2 is the XRD analysis of the freshly prepared Ni-Fe/Al_2O_3 catalyst. There is evidence of the Al_2O_3 support in each of the samples at 2θ diffraction peaks at 37.5°, 45.5° and 67°. The most significant difference between the reduced Ni-Fe catalyst and the used catalyst after pyrolysis/CVD of polypropylene and polystyrene experiments is the presence of a large 2θ peak at 26.5°, characteristic of graphitic carbon;[50] this suggests that crystalline carbon deposits were formed during pyrolysis/CVD of both polypropylene and polystyrene. The XRD data for the freshly prepared and used catalysts exhibit peaks corresponding to a Ni-Fe alloy at 45°, 51° and 75°2θ. The 2θ peak at 45° could also result from pure Ni or Fe, and the 2θ peak at 51° could be caused by pure Ni metal. Interesting features to note are the double peaks present at 2θ ~45°, ~51° and 75° for the freshly prepared Ni-Fe/Al_2O_3 catalyst but absent for the used catalysts obtained with polypropylene and polystyrene processing.

This could indicate that (i) metal oxides are still present within the catalyst, even after reduction [51] or (ii) Ni-Fe alloys of different molar ratios are present. Taking the latter case, Zhang et al.[52] compared XRD spectra of bimetallic Ni-Fe catalysts before and after reduction. Prior to reduction, only one broad peak was present at ~45°, which was attributed to kamacite (a Ni-Fe alloy containing an approximate molar ratio of Fe/Ni 94:6). After reduction, the broad peak was split into two narrower peaks, similar to those shown in Figure 2, caused by the presence of both kamacite and $Fe_{0.64}Ni_{0.36}$ alloy. The removal of the double peaks in the XRD profiles obtained with the used catalysts from pyrolysis/CVD of polypropylene and polystyrene suggests that the double peaks was caused by metal oxides. Hydrogen produced during the plastic pyrolysis process would have further reduced the catalyst during CVD, thus the metal oxide peaks would not be present.

Further analysis of the catalyst chemistry was undertaken using Fe K-edge Extended X-ray Absorption Fine Structure (EXAFS) and confirmed the reduction of the catalyst. In addition, Fe XANES (X-ray Absorption Near Edge Structure) also confirmed that the catalyst was a FeNi alloy rather than zero valent metallic Fe (Figure 3(a). EXAFS results also showed that the average coordination environment of Fe was identical in the used catalyst from polypropylene and polystyrene processing (PP-CNT and PS-CNT samples. Figure 3(b) shows the data and fit for the catalyst used with polypropylene (PP-CNT) are in good agreement in Fourier-transformed space. Figure 3b, showing the magnitude of the EXAFS FT, does not include the contribution of paths used for fitting the EXAFS data. Table 4 shows the best fit values for EXAFS modelling of the catalyst after pyrolysis/CVD with polypropylene. Quantitative modelling of the Fe EXAFS data shows 2.3 ± 0.3 Fe atoms and 4.6 ± 0.6 Ni atoms around the Fe central atom at 2.46 ± 0.02 and 2.53 ± 0.02 Å respectively. Bond distances for Fe and Ni atoms are in good agreement with $FeNi_2$ catalyst formation.[53] However, a Ni coordination number of 4.6 ± 0.6 suggests the presence of a small fraction of a $FeNi_3$phase in addition to $FeNi_2$.

In summary, EXAFS suggests the presence of primarily (about 70-80%) $FeNi_2$ with a small fraction (20-30%) of $FeNi_3$. However, it is also possible to have a local heterogeneity of the two phases such that the two FeNi phases are not homogeneously distributed. A previous study has shown formation of $FeNi_3$ catalyst using High Resolution Transmission Electron Microscopy (HRTEM) lattice fringes.[54] It is important to note that XAFS provides averaged, bulk information while HRTEM provides spatially localised information. Hence,

finding $FeNi_3$ using HRTEM is within the realm of results presented in this study, which suggests that the catalyst forms an Fe-Ni_2 alloy after the pyrolysis/CVD process.

3.3. Characterisation of catalyst carbon deposits

The carbon deposits on the catalyst produced via the pyrolysis/CVD process result in high yield (shown in Table 3), at 33.5 wt.% for the waste polypropylene processing and 29.5 wt.% for the waste polystyrene. The wide range of hydrocarbons produced from the pyrolysis of the plastics are decomposed at the Ni and Fe metal particles of the Ni-Fe/Al_2O_3 catalyst to produce carbon deposits on the catalyst surface and also hydrogen. Detailed characterisation of the carbon deposits on the Ni-Fe/Al_2O_3 catalyst after pyrolysis/CVD processing of the waste polypropylene and polystyrene, particularly using advanced analytical techniques, will reveal, not only the presence of carbon nanotubes, but also their quality and properties.

3.3.1. Temperature programmed oxidation (TPO)

Temperature programmed oxidation of the carbon deposits on the used catalyst after pyrolysis/CVD processing of the waste polypropylene and polystyrene was undertaken using thermogravimetric analysis with an air atmosphere. The derived thermograms are shown in Figure 4. TPO is used as an analytical technique to differentiate between amorphous and more graphitic carbons, which include both carbon nano-fibres and carbon nanotubes.[36,51,55] Amorphous carbons are more easily oxidised at lower temperature (~400 °C) than the less reactive, more graphitic filamentous carbon nano-fibres and carbon nanotubes which oxidise at higher temperature (>550 °C), thereby, two peaks of mass loss are produced during the TPO analysis. The TGA-TPO thermograms for the catalyst carbon deposits (Figure 4(a)) show a total mass loss due to carbon oxidation of the used catalysts of 44 wt.% for polypropylene processing and 41 wt.% for polystyrene processing. In contrast, the commercial MWCNTs showed a 99 wt.% mass loss due to carbon oxidation. This was because the sample mass for the carbon deposits derived from pyrolysis/CVD processing of the waste plastics, also included the Ni-Fe/Al_2O_3 solid

catalyst. The commercial MWCNTs were almost exclusively carbon (>98% reported carbon content) having been subject to hydrochloric acid demineralisation after CVD production. Consequently, the TGA-TPO resulted in almost complete oxidation of the sample.

The DTG-TPO thermogram shown in Figure 4(b), represents the derivative of the TGA, or rate of mass loss. There was no evidence of oxidation at a temperature of ~400 °C for any of the carbon samples. Instead, all three samples have a peak mass loss at a temperature above 550 °C, indicating that there is only graphitic carbon present. The commercial MWCNT (Com-MWCNT) sample showed a mass loss peak at a lower temperature than both PP-CNT and PS-CNT suggesting the carbon is more reactive, which indicates the presence of nanotubes with smaller diameters as reported by Yao et al.[56] The narrow peak also suggests a small diameter size distribution, in contrast to the carbon oxidation in relation to the carbons produced from polypropylene and polystyrene processing. It is likely therefore, that there is a larger diameter distribution of the filamentous carbons compared with the commercial MWCNTs sample. Peak temperatures for the mass loss for the commercial MWCNTs was 559 °C, whereas the carbon deposits produced from polypropylene and polystyrene processing were 612 °C and 644 °C, respectively. The similar peaks and shapes of the TPO-DTG mass loss thermograms for the polypropylene and polystyrene feedstocks indicate that both contained a high degree of graphitic carbon and structures with similar oxidation temperatures.

3.3.2. Scanning electron microscopy

Scanning electron microscopy (SEM) was conducted to further characterise the carbon deposits on the used catalysts after pyrolysis/CVD processing. The freshly prepared Ni-Fe/Al_2O_3 catalyst was also examined. The SEM images are shown in Figure 5. The freshly prepared Ni-Fe/Al_2O_3 catalyst exhibited a coarse granular structure with smaller irregular shaped particles on the surface. In contrast, the used catalysts after pyrolysis/CVD of the waste plastics showed a large amount of long entangled, string-like filamentous deposits covering the surface of the catalysts. There was little evidence of amorphous type carbon on the used catalysts produced with either waste plastic. The carbon deposits on the used catalyst derived from polypropylene processing appeared longer, thinner and more

uniform in both length and diameter. Whereas the filamentous carbons produced from polystyrene processing appeared shorter, more entangled with a range of different lengths and diameters and were irregular in shape compared to those produced with polypropylene. In addition, the carbons produced with polystyrene contained significant amounts of globular carbon clusters rather than long narrow filaments of carbon.

3.3.3. Transmission electron microscopy

Due to the nature of SEM, it is difficult to determine whether the filamentous carbon produced from the pyrolysis/CVD processing of the waste plastics was in the form of carbon nanotubes or solid nano-fibres. Therefore, further characterisation of the carbon filamentous deposits using high-resolution TEM was carried out. TEM micrographs of the catalyst carbon deposits produced from polypropylene and polystyrene are shown in Figure 6. Also shown, for comparison, are TEM micrographs of com-MWCNT.

Figure 6 shows that the carbon filaments observed in the SEM micrographs of Figure 5 are indeed multi-walled carbon nanotubes. The MWCNTs derived from polypropylene were several micrometres in length with thick walls linked to the larger diameter of the carbon nanotube. MWCNTs derived from polystyrene, were also long (several μm in length) with larger diameters. However, polystyrene-derived MWCNTs include highly irregular and coiled MWCNTs with defects (Figure 6). The larger diameter of the MWCNTs produced from polypropylene and polystyrene has been linked to the larger number of graphene layers in the wall of the nanotube.[57] The commercial MWCNTs, in contrast, are smooth walled with thinner walls, linked to the smaller number of graphene layers in the nanotube wall. The number of graphene layers was determined from the TEM images and for polypropylene, there were approximately 30 graphene layers in the wall and ~27 graphene layers for the polystyrene derived MWCNTs whereas for the commercial MWCNTs, there were only ~12 graphene layers (Figure 6). In addition, the diameters of the com-MWCNT are much smaller (~10 nm) compared to the polypropylene and polystyrene derived MWCNTs, which both have MWCNT diameters of ~50 nm. Also, the commercial MWCNTs sample is much more homogeneous, with a considerably smaller diameter range compared with the MWCNTs obtained from pyrolysis/CVD processing of the waste plastics.

The larger diameter and large number of graphene layers in the nano-tube wall may be linked to the larger nano-particle size of the active catalyst metal, (Ni and Fe). Catalyst particle size has been shown to be an important factor in determining CNT diameter.[58-60] The MWCNTs produced from the waste plastics show the presence of nanometre sized metal particles within, or at the tip of several carbon nano-tubes (Figure 6). However, for the commercial MWCNTs, these metal particles are generally not present. This is due to the post-production process step of acid demineralisation of the CVD catalysts using hydrochloric acid.

The characteristics of the MWCNTs as shown by the TPO, SEM and TEM results shows that the MWCNTs obtained from pyrolysis/CVD of polypropylene were significantly different from those obtained from polystyrene processing. The pyrolysis of polypropylene results in thermal degradation of the linear and branched aliphatic structured polymer to produce a range of hydrocarbons which are mainly n-alkanes with a molecular weight range from C_1— C_{60}, and also at lower concentrations, alkenes and alkadienes.[24] The pyrolysis of polystyrene produces an aromatic, mainly liquid, product derived from the thermal degradation of the aromatic structured polymer producing mainly styrene, but also styrene oligomers, benzene, toluene, xylene and alkylated benzenes.[24] For the pyrolysis/CVD process used in this work, the product hydrocarbons from pyrolysis of polypropylene or polystyrene do not condense but pass as a suite of different hydrocarbon gases/vapours directly to the CVD reactor containing the catalyst. As such the different gases/vapours produced from polypropylene and polystyrene will influence the characteristics of the product MWCNTs.

Previous studies have also shown that distinct differences in CNT characteristics are produced depending on the type of plastic used in the pyrolysis/CVD process. For example, Chung et al.[61] used a quartz vacuum pyrolysis/catalytic reactor system where the plastic was mixed with iron nano-particle catalyst. They reported that the product MWCNTs produced from polystyrene had larger diameters with thicker graphene nano-tube walls compared to MWCNTs produced from polypropylene. Aboul-Enein et al.[62] produced MWCNTs from several different waste plastics using a pyrolysis/catalytic (CVD) reactor system. Pyrolysis of the plastics produced a range of different hydrocarbons which were passed to a condenser to remove heavier molecular weight components and the non-condensable gases were passed to a CVD reactor to produce MWCNTs on a Ni-

Mo/Al_2O_3 catalyst. They reported that polypropylene produced a higher yield of MWCNTs compared to polystyrene which was linked to the higher yield of non-condensable gases produced compared to polystyrene which produced a mainly liquid product and consequently, lower gas yield and lower MWCNTs production. Processing of polystyrene also produced MWCNTs which were of poor quality, showing structural defects(as was also shown in this work). Veksha et al.[19] also used a pyrolysis/CVD system with an intermediate condenser to remove heavier molecular weight hydrocarbon products for the investigation of different plastics for MWCNTs production. They reported high yields of MWCNTs for the processing of polypropylene, but negligible yields for polystyrene due to the removal of hydrocarbons in the intermediate condensation step.

The MWCNTs produced from the pyrolysis/CVD processing of the waste plastics appear to be of inferior quality compared with the commercial MWCNTs. The commercial MWCNTs have a long length, a small and narrow range of diameter, smaller number of graphene layers in the nano-tube wall, absence of catalyst metal impurities and a more uniform smooth shape. In contrast, the plastic derived MWCNTs are entangled, have larger diameter, are thicker walled, and a wider range of nano-tube diameters containing numerous catalyst metal particles. However this is not unexpected, as the commercial MWCNTs were synthesised from pure volatile hydrocarbon gas feedstock and using a more uniform nano-sized metal particle CVD catalyst. Additionally, the commercial MWCNTs underwent a purification step in the production process to remove the residual catalyst.

3.3.4. Optical Raman spectroscopy

The quality of the MWCNTs produced as catalyst carbon deposits from the processing of the waste plastics in terms of the degree of graphitisation and presence of defects was determined using optical Raman spectroscopy. The resultant Raman spectra are shown in Figure 7, which shows three distinct bands at wavelengths of 1343 cm^{-1}, 1572 cm^{-1} and 2683 cm^{-1}. The band at wavelength 1343 cm^{-1} corresponds to the G-band, which indicates the degree of graphitisation of the sample (i.e. *Graphitisation* equates to the G-band); the band at 1572 cm^{-1} is assigned to the D band, which is caused by defects (i.e. *Defects*

equates to the D-band) at the borders of crystalline areas; and the band at 2683 cm^{-1} is characteristic of the G' band, an overtone of the D-band, which is caused by the second-order two-phonon scattering process.[63] Unlike the *D*-band, however, it is not activated by being close to a defect. Two-phonon scattering processes only occur in amorphous carbon, therefore the presence of the G' band can be used as an indicator of the degree of long-range order of CNTs.[64] If these peaks are present in a Raman spectra, then it indicates that CNTs have been formed within a carbon deposit. Ratios of the (i) G and D band (I_D/I_G) and (ii) G' and G band (I^0_G/I_G) are commonly used to quantify the (i) degree of defects within and crystallinity of CNTs and (ii) long-range order of the CNTs.[65-67] The ratio of the *G* and *D* band (I_D/I_G) [62] and the width of the *G*-band [68] are commonly used to assess the degree of defects within a CNT sample. The smaller the I_D/I_G ratio, the more defect-free the sample, with a value <1 representing a higher degree of graphitisation and lower defect concentration. In contrast, as high an I^0_G/I_G ratio as possible is desired, as this indicates a higher degree of long range order.

Figure 7 shows that there is clear evidence of graphitic crystallinity for the carbons derived from the pyrolysis/CVD processing of both the polypropylene and the polystyrene. The G-band at the Raman spectra of wavelength 1343 cm^{-1}, exhibited a strong intensity and the I_D/I_G ratios were <1, indicating a high degree of graphitisation and low amount of defects in MWCNTs produced from both polypropylene and polystyrene. The stronger intensity of the G-band and the I_D/I_G ratio of 0.76 for the MWCNTs produced from polypropylene represented a higher degree of graphitisation and lower amount of defects compared to the MWCNTs derived from polystyrene (I_D/I_G ratio of 0.78). The commercial MWCNTS produced an I_D/I_G ratio of 0.73 suggesting they had the highest degree of graphitisation. However, the width of the *G*-band peak followed the order of, polypropylene-MWCNTs < commercial-MWCNTs < polystyrene-MWCNTs suggesting that the polypropylene-MWCNTs had the highest degree of graphitisation. This is in contrast to the I_D/I_G ratio data which suggested that the commercial MWCNTs had the highest degree of graphitisation.

Other researchers investigating the production of MWCNTs from waste plastics have also reported I_D/I_G ratio as an indication of the degree of graphitisation and purity. Mishra et al.,[65] reported on the production of MWCNTs using a pyrolysis/CVD reactor with waste polypropylene with a Ni catalyst held at different temperatures. Raman spectra of the CNTs produced at different temperatures were compared at a wavelength

of 532 nm. They reported the Raman spectroscopy I_D/I_G ratios of 0.57 at a catalyst temperature of 800 °C, lower than the I_D/I_G ratio reported here, indicating a higher quality of MWCNTs. Cai et al.[69] used Raman spectroscopy to determine the quality of MWCNTs produced from waste polypropylene. The I_D/I_G ratio reported for a catalyst temperature of 800 °C was 0.86, which indicates that their CNTs had a lower degree of graphitisation compared to the MWCNTs produced in this work. Yao et al.[70] investigated the use of real world plastics for CNT synthesis using a variety of catalysts, and reported an I_D/I_G ratio of 0.43 for a Ni-Fe alumina catalyst. Acomb et al.[18] used Raman spectroscopy to characterise MWCNTs obtained from pyrolysis/catalysis (CVD) of polyethylene in a two stage reactor system with a Fe/Al_2O_3 catalyst. The reported Raman spectroscopy analysis for the I_D/I_G ratio was 0.51 at a catalyst temperature of 800 °C. Moo et al.[71] investigated the production of MWCNTs using waste polyethylene, polypropylene and a mixture of waste plastics with a $NiO/CaCO_3$ catalyst in a two-stage pyrolysis/catalytic (CVD) reactor. They reported a significantly higher quality of MWCNTs obtained at a catalyst temperature of 800 °C with a I_D/I_G ratio of 0.38 indicating the production of high quality, highly graphitic MWCNTs with low defects. Significantly inferior MWCNTs as determined from Raman spectroscopy I_D/I_G ratio, in terms of the degree of graphitisation and the presence of defects have been reported by several authors at catalyst temperatures less than 800 °C.[18,19,65,71] Therefore, indicating that the CVD catalyst temperature should be not less than 800 °C, as used in this work.

3.3.5. X-ray Raman scattering spectroscopy

XRS spectroscopy was used to compare and contrast the local structure of PP, PS and COM-MWCNTs. As stated earlier, XRS spectroscopy allows for the element-specific characterisation of low-Z elements (e.g., C) using hard X-rays. The use of hard X-rays allows one to measure the bulk local chemistry of carbon within the sample. In this case, XRS was used to give further insight into the aromaticity and functionality of the produced MWCNTs. XRS provides advantages over other spectroscopy techniques for this purpose.[47] Optical Raman spectroscopy does not provide information regarding the presence of non-aromatic carbon functionality and, in this case, provides conflicting metrics for the total degree of aromatisation of the sample (i.e., G-band FWHM vs I_D/I_G).

Other bulk carbon spectroscopy (e.g., 13C-NMR) would be challenging due to magnetic interference from residual Fe/Ni catalyst. Alternatively, soft X-ray techniques such C *K*-edge NEXAFS are surface limited and may also suffer from spectral artefacts due to self-absorption and the presence of residual catalyst.

Carbon *K*-edge XRS spectra of the carbon deposits obtained from the pyrolysis/CVD processing of PP and PS and shown with the spectrum of the commercial MWCNT product in Figure 8(a). Peaks 1 and 3 correspond to the 1s-π* (285 eV) and 1s-σ* (292 eV) core electron transitions of the aromatic carbon atom, respectively.[72,73] Although the spectral pattern of the pyrolysis/CVD-derived MWCNT spectra have similarities with the commercial product, significant differences are observed, such as broadening of features 1 & 3, and increased intensity in region 2 for the pyrolysis/CVD carbon deposits. In order to quantify the qualitative observations described above, spectral deconvolution of the background subtracted and normalised data was performed using Gaussian functions. In addition to providing fingerprinting information regarding the ratios of aromatic and aliphatic/graphitic components, modelling the experimental data using Gaussian functions with centroid fixed at transition energies for known carbon functionalities provide relative abundance of different carbon moieties within the sample (Table 2).[47,74,75] The results of the fitting for COM-CNT PP-CNT and PS-CNT are shown in Figures 7(b) - 7(d); the resulting peak areas (A_g) and full-width-half-maxima (FWHM) are listed in Table 5.

The aromatic 1s-π* region of the C *K*-edge spectra shows significant broadening between the samples. Broadening of the 1s-π* electron transition in condensed aromatic materials, such as these, has been shown to correspond to reduced aromatic condensation and increased local structural disorder within the sample. [76] Similarly, increased intensity at the 1s-π* aromatic transition may be used as a metric for determining the total aromaticity of the sample. When compared to COM-CNT, PP-CNT shows a similar FWHM, however PP-CNT shows a significant increase (ca. 16%) in peak area. The increased peak area for PP-CNT over COM-CNT indicates increased peak intensity and, therefore, aromaticity.[77,78] This result confirms the comparison of optical Raman G-band FWHM, which shows that PP-CNT has the highest aromaticity. PP-CNT also displays increased intensity at the aromatic 1s-σ* and a higher degree of fine structure after 292 eV than either COM-CNT or PS-CNT, which supports the conclusion that PP-CNT displays more local structural ordering. In contrast, PS-CNT shows a 'flatter' 1s-σ*

transition, which is characteristic of less well-ordered aromatic carbon systems. Furthermore, the FWHM of the 1s-π* aromatic transition is larger (ca. 6%) than either PP-CNT or COM-CNT, which indicates that PS-CNT has a lower degree of aromatisation.[78-80] Similarly, the reduced intensity of the 1s-π* transition also indicates lower aromaticity than either PP-CNT or COM-CNT.

XRS spectroscopy allows an in-depth analysis of the carbon chemical bonding beyond aromatic species by investigating the energy region between the 1s-π* and 1s-σ* electron transitions (i.e., 286 – 290 eV). In this region (labelled 2 in Figure 8(a)), three carbon functionalities were fitted: (i) Aryl aromatic carbon groups C=C-X (G2; 286.0 - 287.4 eV) (ii) carboxyl functionalities (G3; 288.0 – 288.7 eV) and (iii) carbonyl functionalities (G4; 289.5 – 290.2 eV). Peak areas correspond to relative concentrations of each carbon functionality within a sample. The peak area for transition G2 remains similar between COM-CNT and PS-CNT, however PP-CNT shows a smaller peak area suggesting that all samples had similar aryl functional concentrations. This is most likely due to reduced FWHM of the 1s-π* transition in PP-CNT because of the presence of fewer aromatic functionalities suggesting that PP-CNT has a higher degree of aromatisation than either PS-CNT or the commercial product. Peak G3 shows higher peak area in both the pyro/CVD carbons than in COM-CNT. This is likely due to the increased presence of oxygen groups in the waste plastic derived carbons than in the commercial product, this is also supported by the TPO measurements.[81-83] The energy position of G3 differs significantly between PP-CNT and PS-CNT, which suggests that carbon oxide functionality present on the pyrolysis/CVD samples may differ between initial plastic feedstocks, perhaps due to differences in the formation mechanisms of CNTs on metal-oxides in the sample. The presence of carbon oxide functionalities in both pyrolysis/CVD derived MWCNTs is likely to increase their reactivity towards oxyphilic elements, which may have advantages for certain applications such as water purification. Finally, peak G4 (~289.7 eV) was assigned to carbonyl functionalities. However, evidence of crystalline carbonyl functionality was not present in the powder XRD patterns, and non-crystalline carbonyl functionalities are likely to have degraded at these pyrolysis temperatures.[84] A well-defined peak can be observed in both Figure 8(c) and Figure 8(d) for PP-CNT and PS-CNT respectively, but is absent in the spectra for COM-CNT. A previous C *K*-edge NEXAFS study found a similar peak in Cr and Fe modified MWCNTs, which is absent in the unmodified

sample.[85] It is possible therefore, that the feature at G4 represents the interaction between MWCNT carbon and the catalyst (e.g. Fe-O-¬C).

Taken together, XRS results suggest that the aromaticity of the measured CNTs falls in the order: PP-CNT > COM-CNT > PS-CNT. In this respect, XRS appears to confirm optical Raman G-band measurements, which suggest that PP-CNT is the most structurally ordered CNT sample. Both PP-CNT and PS-CNT contains a higher concentration of carbon oxides (e.g. carbonyl species) than the COM-CNT. The presence of carbon oxides are likely to increase the reactivity of both PP-CNT and PS-CNT towards oxyphilic elements. A feature at ca. 289.7 eV in the C *K*-edge spectrum for PP-CNT and PS-CNT is likely to represent the interaction between the formed carbon and the catalyst. This interaction is more significant in the spectrum for PP-CNT than PS-CNT. XRS spectroscopy represents a route for bulk carbon spectroscopy for carbon nanotubes not possible using ^{13}C-NMR or C *K*-edge NEXAFS.

The results have shown that MWCNTs can be produced from polypropylene and polystyrene using a N-Fe/Al_2O_3 catalyst. Bimetallic Ni-Fe catalysts have been shown to have a higher catalytic activity towards CNT production compared to Ni- and Fe-based catalysts. [27] The presence of the Ni and Fe in the form of an alloy has been suggested as the active phase for the enhanced growth of MWCNTs from methane. [86] Here we have also shown that an Ni-Fe alloy is the key for enhanced MWCNTs formation and growth, and that the active metal species that promotes MWCNTs production are due to the presence of mainly $FeNi_2$ (~70-80%) with a smaller amount of $FeNi_3$ (~20-30%). Polypropylene produced CNTs which were of higher quality than those produced from polystyrene, in terms of the degree of graphitisation and the amount of defects in the MWCNTs. The thermal degradation of the polypropylene in the first stage pyrolysis will produce a range of low molecular weigh alkanes and alkenes produced by the random and beta scission of the polyethylene polymer. However, for polystyrene, the thermal degradation products from the first stage pyrolysis are dominated by aromatic compounds produced from the chain-end scission of the polymer, producing smaller aromatic compounds, mostly styrene, but also other aromatic compounds such as benzene and xylene.

When these hydrocarbon volatiles are passed into the second stage catalytic reactor, held at 800 °C, the hydrocarbons will undergo further thermal cracking to produce more light hydrocarbons.[87] Additionally, there will be catalytic cracking of larger molecules to produce further smaller molecular weight hydrocarbons. In terms of CNT formation, these lower molecular weight hydrocarbons will react with the different Ni-Fe metal species, i.e. the $FeNi_2$ and $FeNi_3$, on the Hi-Fe/Al_2O_3 catalyst to produce MWCNTs. The role of the $FeNi_2$ and $FeNi_3$ nanoparticle metal species is to cleave the carbon-carbon and carbon-hydrogen bonds of the lower molecular weight hydrocarbons to produce hydrogen and carbon atoms which are dissolved into these metal species and diffuse throughout the nanometal particles.[26] As the concentration of carbon in the metal increases to saturation, precipitation of the carbon takes place and the MWCNTs are formed.[26,88] The formation and growth of the MWCNTs involves either base growth or tip growth mechanism and is dependent on the strength of interaction of the metal species and the support material. For weak interaction between metal and support, tip growth occurs, where the metal particle lifts from the catalyst surface as the MWCNTs grow. Alternatively, for strong metal-support interaction, base growth occurs, where the metal particle is held at the catalyst support surface and the MWCNTS grow away from the metal particle. [88] During the hydrocarbon catalytic decomposition to produce carbon MWCNTs, the hydrogen that is formed may also enhance CNT formation since hydrogen has been shown to moderate the rate of carbon deposition and minimise catalyst deactivation.[89]

The mechanism for MWCNTs formation described will be influenced by the hydrocarbon precursors generated from the thermal and catalytic decomposition of the polypropylene compared with polystyrene. Decomposition of polypropylene facilitates formation of light hydrocarbons such as methane, ethane, ethene, propane and propene where carbon-carbon and carbon-hydrogen bond dissociation energy is lower and cleaving is readily achieved producing the carbon for MWCNTs growth. However, for polystyrene decomposition, light hydrocarbons will be formed and produce the MWCNTs as described before. However, aromatic hydrocarbons are also produced, such as styrene, benzene and toluene, where bond dissociation energies are higher and bond cleaving is more difficult, with the potential to also produce irregular MWCNT's growth.[26]

Using waste plastics as a feedstock source for the production of MWCNTs has advantages in that the plastic resource is derived from the processing of fossil crude

petroleum and thereby mitigates against the depletion of fossil fuels. However, as we show here, the MWCNTs produced from waste plastics are of lower quality compared to commercially produced carbon nanotubes produced from pure hydrocarbons. Post-consumer plastics are not pure polymers, often containing a range of additives used to improve the properties of the plastic, such as fire retardants, colourants, anti-oxidants, inorganic fillers etc. There may also be contamination from other plastics from the sorting and recycling process of the waste plastics, which may also include some inorganic contamination. Consequently, these additives and contaminants will detrimentally influence the formation of the MWCNTs in the pyrolysis/CVD process, producing MWCNTs with defects and contaminants such as the presence of oxygenated species, as was shown in this work. However, there are further issues to be resolved to take the process forward, including the logistics of producing a homogeneous plastic waste stream as the feedstock for the process including the collection and sorting of the post-consumer plastic waste.

Although of lower quality, the MWCNTs produced are of sufficient quality and in high yield and have potential to be used in some lower-end commercial industrial applications. For example MWCNTs have been used as additives for tyre manufacture, for energy storage [3] and used as strengthening reinforcement in plastics composite material.[90] The quality and specifications of such MWCNTs are lower than that required for higher end applications such as for use in transistors for microelectronics and for biosensors and medical devices. A recent study by Ahamed et al. [91] has demonstrated the viability of producing MWCNTs from waste plastics. They reported on a life cycle analysis (LCA) of processing different compositions of waste plastic to produce pyrolysis oil and multi-walled carbon nanotubes. They reported that the integrated process produces various environmental benefits in addition to producing a high value MWCNTs product, providing additional revenues for the plastics pyrolysis plant operators. However, further work is required to determine the market demand for MWCNTs prodiuced from waste plastics and to match the characteristics of the produced MWCNTs to the specific required specifications of the end-use application.

4. CONCLUSIONS

MWCNTs were successfully synthesised from two different waste plastics, polypropylene and polystyrene, using a two-stage pyrolysis/CVD process with a bimetallic Ni-Fe/Al_2O_3 catalyst. Extended X-ray Absorption Fine Structure (EXAFS) analysis of the used Ni-Fe/Al_2O_3 catalyst suggested that the active metal phase was an alloy consisting of mainly (~70-80%) $FeNi_2$ with a smaller amount of $FeNi_3$ (~20-30%). The used catalysts showed clear evidence of high levels of carbon deposits on the catalysts used in the waste plastics pyrolysis/CVD experiments. The plastics produced similar temperature programmed oxidation characteristics and carbon deposit yields, 33.5 wt.% for polypropylene and 29.5 wt.% for polystyrene. Scanning electron microscopy images showed the presence of long entangled filamentous carbon deposited on the catalysts during the pyrolysis/CVD process. Transmission electron microscopy images clearly showed that the filamentous carbons were MWCNTs for both polypropylene and polystyrene, however there was also the presence of significant irregular shaped MWCNTs, which was more pronounced for the polystyrene derived MWCNTs. There was a broader diameter distribution linked to the number of graphene layers in the CNT wall for both plastics compared to the commercial MWCNTs; which is likely to be due to the non-uniform catalyst nano-particle active metal size of the prepared Ni-Fe/Al_2O_3 catalyst. Optical Raman spectroscopy showed that catalyst carbon deposits produced from both plastics had high purity and crystallinity. However, the MWCNTs produced from polypropylene showed a higher degree of graphitisation and lower amount of defects compared to the MWCNTs derived from polystyrene, based on the stronger intensity of the G-band and lower I_D/I_G ratio .X-ray Raman scattering spectroscopy was used to compare bulk carbon functionalities of the MWCNTs. It was found that the MWCNTs obtained from polypropylene and polystyrene both contained higher concentrations of oxygenated functional groups (e.g. alkyl, carboxyl) than the commercial MWCNTs due to the presence of impurities (e.g. oxygen containing plastics). The results from this study provide evidence that plastics with different chemical structures can be used to produce valuable MWCNTs of a similar quality, which suggests that plastics do not need to be sorted prior to the pyrolysis/CVD thermal treatment process.

ACKNOWLEDGEMENTS

We gratefully acknowledge the support of the UK Engineering & Physical Sciences Research Council (EPSRC) for research scholarships for KA and for LJRH via the EPSRC Centre for Doctoral Training in Bioenergy (EP/L014912/1).

REFERENCES

[1] S. Iijima, Helical microtubules of graphitic carbon, Nature 354 (1991) 56–58.

[2] M. F. De Volder, S. H. Tawfick, R. H. Baughman, A. J. Hart, Science 64 (2013) 219–253.

[3] S. Kumar, M. Nehra, D. Kedia, N. Dilbaghi, K. Tankeshwar, K. H. Kim, Progress in Energy and Combustion Science 64 (2018) 219–253

[4] H. He, L. A. Pham-Huy, P. Dramou, D. Xiao, P. Zuo, C. Pham-Huy, BioMed Research International 2013 (2013).

[5] M. Kumar, Y. Ando, Journal of nanoscience and nanotechnology 10 (2010) 3739–3758.

[6] Y. Zhang, C. Wu, M.A. Nahil, P.T. Williams, , Energy and Fuels 29 (2015) 3328–3334.

[7] J. Zhu, J. Jia, F. L. Kwong, D. H. L. Ng, S. C. Tjong, Biomass and Bioenergy 36 (2012) 12–19.

[8] N. A. Fathy, RSC Advances 7 (2017) 28535–28541.

[9] M. G. S. Bernd, S. R. Bragança, N. Heck, L. C. d. S. Filho, Journal of Materials Research and Technology 6 (2017) 171–177.

[10] W. Gindl-Altmutter, J. Köhnke, C. Unterweger, N. Gierlinger, J. Keckes, J. Zalesak, O. J. Rojas, Composites Part A: Applied Science and Manufacturing 121 (2019) 175–179.

[11] J. E. Omoriyekomwan, A. Tahmasebi, J. Zhang, J. Yu, Energy Conversion and Management 192 (2019) 88–99.

[12] Plastics – the facts PlasticsEurope, Brussels, 2020.

[13] R. Geyer, J.R. Jambeck, K.L. Law. Science Advances, 3(7), (2017), Sciadv1700782.

[14] European Commission, A strategy for plastics in a circular economy, COM(2018) 28 Final. 16.1.2018. European Commission, Brussels, 2018.

[15] Plastics the Facts 2017, PlasticsEurope, Brussels, 2017.

[16] C. Zhuo, Y. A. Levendis, Journal of Applied Polymer Science 131 (2014). DOI: 10.1002/APP.39931

[17] A. Bazargan, G. McKay, Chemical Engineering Journal, 195, 377-391, 2012

[18] J. C. Acomb, C. F. Wu, P. T. Williams, Journal of Analytical and Applied Pyrolysis 113 (2015) 231–238.

[19] A. Veksha, A. Giannis, V. W. Chang, Journal of Analytical and Applied Pyrolysis 124 (2017) 16–24.

[20] J. Liu, Z. Jiang, H. Yu, T. Tang, Polymer Degradation and Stability, 96(10), (2011) 1711-1719.

[21] A.A. Aboul-Enein, A.E. Awadallah, Chemical Engineering Journal, 354, (2018) 802-816.

[22] N. Borsodi, A. Szentes, N. Miskolczi, C. Wu, X. Liu. Journal of Analytical and Applied Pyrolysis, 120, (2016) 304-313.

[23] C. Muhammad, J.A. Onwudili, P.T. Williams. Energy & Fuels, 29, (2015) 2601-2609.

[24] P.T. Williams. Yield and composition of gases and oils/waxes from the feedstock recycling of waste plastic (Chapter 11). In, Feedstock Recycling and Pyrolysis of Waste Plastics. Schiers J. and Kaminsky W., John Wiley & Sons Ltd, Chichester, 285-314, 2006

[25] Y.H. Cheung, S. Jou, Materials Chemistry, Physics, 92 (2005) 256-259.

[26] N. Cai, X. Li, S. Xia, L. Sun, J. Hu, P. Bartocci, F. Fantozzi, P.T. Williams, H. Yang, H. Chen. Energy Conversion Management, 229 (2021) 113794

[27] D. Yao, C.H. Wang, Applied Energy 265 (2020) 114819

[28] V. Jourdain, C. Bichara, Carbon 58 (2013) 2-39.

[29] J.C. Acomb, C. Wu, P.T. Williams, Applied Catalysis B: Environmental, 180 (2016) 497-510.

[30] W.W. Liu, A. Aziz, S.P. Chai, Mohamed A.R., Journal Nanomaterials (2013) 592464, 1-8.

[31] C.J. Lee, J. Park, A.Y. Jeong, Chemical Physics Letter, 360 (2002) 250-255.

[32] S. Ratkovic, D. Vuljicic, E. Kiss, G. Boskovic, O. Geszti, Materials, Chemistry, Physics 129 (2011) 398-405.

[33] D.A. Kutteri, I.W. Wang, A. Samanta L. Li, J. Hu., Catalysis Science Technology, 8 (2018) 858-869

[34] D. Yao, C. Wu, H. Yang, Y. Zhang, M.A. Nahil, Y. Chen, P.T. Williams, H. Chen, Energy Conversion Management, 148 (2017) 692-700.

[35] D. Yao, H. Yang, Q. Hu, Y. Chen, H. Chen, P.T. Williams, Applied Catalysis B: Environmental, 280 (2021) 119413.

[36] Wu C., Williams P.T., Applied Catalysis B: Environmental, 96, (2010) 198-207.

[37] J. H. Lehman, M. Terrones, E. Mansfield, K. E. Hurst, V. Meunier.. *Carbon*, 49(8) (2011) 2581–2602.

[38] Nicholls R.J., Aslam Z., Sarahan M.C., Sanchez A.M., Dillon F., Koos A.A., Nellist P.D., Grobert N., Phys. Chem Phys. Chem, 17, (2015) 2137-2142.

[39] P. Gueriau, J.-P. Rueff, S. Bernard, J. A. Kaddissy, S. Goler, C. J. Sahle, D. Sokaras, R. A. Wogelius, P. L. Manning, U. Bergmann, L. Bertrand, Analytical Chemistry 89 (2017) 10819–10826.

[40] D. Ketenoglu. Instrumentation Science & Technology, (2020) doi.org/10.1080/10739149.2020.1864742

[41] R.S. Kumar, M.G. Pravica, A.L. Cornelius, M.F. Nicol, M.Y. Hu, P.C. Chow. Diamond and Related Materials, 16, (2007), 1250-1253.

[42] C. J. Sahle, A. Mirone, J. Niskanen, J. Inkinen, M. Krisch, S. Huotari, Journal of Synchrotron Radiation 151 (2015) 105–120.

[43] J. Stöhr, Analysis of K-Shell Excitation Spectra by Curve Fitting, in: NEXAFS, Spectroscopy, Springer Berlin Heidelberg, Berlin, Heidelberg, 1992, pp. 211–238.

[44] M. Newville, A. Ingargiola, T. Stensitzki, D. B. Allen, LMFIT: Non-Linear Least-Square Minimization and Curve-Fitting for Python, Zenodo (2014).

[45] D. Solomon, J. Lehmann, J. Wang, J. Kinyangi, K. Heymann, Y. Lu, S. Wirick, C. Jacobsen, Science of the Total Environment 438 (2012) 372–388.

[46] K. Heymann, J. Lehmann Johannes, D. Solomon, M. W. Schmidt, T. Regier, Organic Geochemistry 42 (2011) 1055–1064.

[47] L. J. R. Higgins, C. J. Sahle, M. Balasubramanian, B. Mishra, Physical Chemistry Chemical Physics (2020).

[48] M. Papagno, A. Fraile Rodriguez, C. O. Girit, J. C. Meyer, A. Zettl, D. Chemical Physics Letters 475 (2009) 269–271.

[49] S. Banerjee, T. Hemraj-Benny, M. Balasubramanian, D. A. Fischer, J. A. Misewich, S. S. Wong, ChemPhysChem 5 (2004) 1416–1422.

[50] A. Yasmin, I. M. Daniel, , Polymer 45 (2004) 8211–8219.

[51] D. Pandey, G. Deo, Journal of Molecular Catalysis A: Chemical 382 (2014) 23–30.

[52] C. Zhang, J. Li, C. Shi, E. Liu, X. Du, W. Feng, N. Zhao, Carbon 49 (2011) 1151–1158.

[53] M.V. Tsodikov, S.S. Kurdymov, G.I. Konstantinov, V.Y. Murzin, O.V. Bukhtenko, Y.V. Maksimov. International Journal of Hydrogen Energy 40, no. 7 (2015): 2963-2970.

[54] N. Cai, H. Yang, X. Zhang, S. Xia, D. Yao, P. Bartocci, F. Fantozzi, Y. Chen, H. Chen, P.T. Williams. Waste Management 109 (2020): 119-126.

[55] P. Wang, E. Tanabe, K. Ito, J. Jia, H. Morioka, T. Shishido, K. Takehira, Applied Catalysis A: General 231 (2002) 35–44.

[56] N. Yao, V. Lordi, S. X. Ma, E. Dujardin, A. Krishnan, M. M. Treacy, T. W. Ebbesen, Journal of Materials Research 13 (1998) 2432–2437.

[57] N. Chiodarelli, O. Richard, H. Bender, M. Heyns, S. De Gendt, G. Groeseneken, P. M. Vereecken, Carbon 50 (2012) 1748–1752.

[58] D. Chen, K. O. Christensen, E. Ochoa-Fernández, Z. Yu, B. Tøtdal, N. Latorre, A. Monzón, A. Holmen, Journal of Catalysis 229 (2005) 82–96.

[59] M. H. Rümmeli, F. Schäffel, C. Kramberger, T. Gemming, A. Bachmatiuk, R. J. Kalenczuk, B. Rellinghaus, B. Büchner, T. Pichler. Journal of the American Chemical Society 129 (2007) 15772–15773.

[60] F. Schäffel, C. Kramberger, M. H. Rümmeli, D. Grimm, E. Mohn, T. Gemming, T. Pichler, B. Rellinghaus, B. Büchner, L. Schultz. Chemistry of Materials 19 (2007) 5006–5009.

[61] Y.H. Chung, Jou S. Materials Chemistry & Physics, 92, 256-259, 2012.

[62] A.A. Aboul-Enein, A.E. Awadallah, A.H. Abdel-Rahman, A.M., Haggar A.M. Fullerenes, Nanotubes and Carbon Nanostructures, 26(2), 443-450, 2018.

[63] C. Wu, M. A. Nahil, N. Miskolczi, J. Huang, P. T. Williams, Environ Sci Technol 48 (2013) 819–826.

[64] R. A. DiLeo, B. J. Landi, and R. P. Raffaelle. *Journal of Applied Physics*, 101:064307, 2007.

[65] N. Mishra, G. Das, A. Ansaldo, A. Genovese, M. Malerba, M. Povia, D. Ricci, E. Di Fabrizio, E. Di Zitti, M. Sharon, M. Sharon. Journal of Analytical and Applied Pyrolysis 94 (2012) 91–98.

[66] R. A. Di Leo, B. J. Landi, R. P. Raffaelle, Journal of Applied Physics 101 (2007) 064307.

[67] Y.A. Kim, T. Hayashi, K. Osawa, M. S. Dresselhaus, M. Endo. *Chemical Physics Letters*, 380(3-4):319–324, 2003.

[68] Y. Kaburagi, A. Yoshida, Y. Hishiyama, Chapter 7 - Raman Spectroscopy, in: M. Inagaki, F. B. T. M. S. Kang, E. of Carbon (Eds.), Materials Science and Engineering of Carbon: Characterization, Butterworth-Heinemann, 2016, pp. 125–152.

[69] N. Cai, S. Xia, X. Zhang, Z. Meng, P. Bartocci, F. Fantozzi, Y. Chen, H. Chen, P. T. Williams, H. Yang. ChemSusChem 13 (2020) 938–944.

[70] D. Yao, Y. Zhang, P.T. Williams, H. Yang, H. Chen. Applied Catalysis B: Environmental 221 (2018) 584–597.

[71] J. G. S. Moo, A. Veksha, W. D. Oh, A. Giannis, W. D. C. Udayanga, S. X. Lin, L. Y. Ge, and G. Lisak. *Electrochemistry Communications*, 101:11–18, 2019.

[72] D. A. Fischer, R. M. Wentzcovitch, R. G. Carr, A. Continenza, A. J. Freeman, Physical Review B 44 (1991) 1427–1429.

[73] R. A. Rosenberg, P. J. Love, V. Rehn, Physical Review B 33 (1986) 4034–4037

[74] D.A. Outka, J. Stöhr, J. Journal of Chemical Physics 88(6) (1988) 3539–3554.

[75] A. Gainar, J.S. Stevens, C. Jaye, D.A. Fischer, S.L.M. Schroeder. Journal of Physical Chemistry B119 (45) (2015) 14373–14381.

[76] U. Bergmann, H. Groenzin, O.C. Mullins, P. Glatzel, J. Fetzer, S.P.P. Cramer, S. P. P. Chemical Physics Letters, 369(1–2), (2003) 184–191.

[77] K. Heymann, J. Lehmann, D. Solomon, M.W.I Schmidt, T.C. Regier. Organic Geochemistry 42(9) (2011) 1055–1064.

[78] D.B. Wiedemeier, S. Abiven, W.C. Hockaday, M. Keiluweit, M. Kleber, C. Masiello, et al. Organic Geochemistry 78 (2015) 135–143.

[79] U. Bergmann, H. Groenzin, O.C. Mullins, P. Glatzel, J. Fetzer, S.P.P. Cramer. Chemical Physics Letters 369 (1–2) (2003) 184–191.

[80] A.E. Pomerantz, N.W. Bostrom, R.L. Kleinberg, E. Crace, T.C. Weng, D. Sokaras, D. Nordlund. Energy & Fuels 33 (2019) 2099–2105.

[81] S. Banerjee, T. Hemraj-Benny, M. Balasubramanian, D. A. Fischer, J. A. Misewich, S. S. Wong. Chemical Communications (2004) 772–773

[82] A. Kuznetsova, I. Popova, J. T. Yates, M. J. Bronikowski, C. B. Huffman, J. Liu, R. E. Smalley, H. H. Hwu, J. G. Chen. Journal American Chemical Society 123 (2001) 10699–10704.

[83] J. Zhong, L. Song, Z.-Y. Wu, S.-S. Xie, M. Abbas, K. Ibrahim, H. Qian. Carbon 44 (2006) 866–872

[84] P.T. Williams, S. Besler, S. Renewable Energy 7(3) (1996) 233–250.

[85] D. Sivkov, O. Petrova, A. Mingaleva, A. Ob'edkov, B. Kaverin, S. Gusev, I. Vilkov, S. Isaenko, D. Bogachuk, R. Skandakov, V. Sivkov, S. Nekipelov. *Nanomaterials 10* (2020) 374.

[86] Y. Li, D. Li, Catalysis Today (162 (2011) 1-48.

[87] D. Yao, H. Li, Y. Dai, C.H. Wang, Chemical Engineering Journal, 2020 #127268.

[88] M. Kumar. Carbon nanotubes- Synthesis and growth mechanism. In Yellampalli S., Nanotechnology and nanomaterials;Carbon nanotubes- Synthesis, characterisation, applications, Intech, 2011.

[89] S. Papari, H. Bamdad, F. Berruti, Materials 14 (2021), 2586.

[90] Wu C., Nahil M.A., Miskolczi N., Huang J., Williams P.T., Process Safety & Environmental Protection, 103, 107-114, 2016.

[91] A. Ahamed, A. Veksha, K. Yin, P. Weerachanchai, A. Giannis, G. Lisak, Journal of Hazaradous Materials, 390 (2020) #121449.

Table 1: Proximate and ultimate analysis of the waste plastics

Plastic	Proximate analysis (wt.%)				Ultimate analysis (wt.%)				
	Moisture	Ash	Volatiles	Fixed carbon	C	H	N	S	O*
Polypropylene	0.2	0.2	99.9	0.1	82.1	14.4	0.0	0.0	3.2
Polystyrene	0.0	0.9	100.0	<0.1	89.0	8.2	0.0	<0.1	2.8

* = by difference.

Table 2: Organic carbon structures with their transitions and energy ranges that were used in Gaussian fitting of XRS spectra.

Carbon form	Bond	Transition	Peak energy (eV)	Gaussian	Ref.
Aromatic C	C=C	1s-π*	284.9-285.5	g1	[31,32]
Aromatic C withsubstituent	C—C–OH C—O R–(C—O)–R	1s-π*	286.0–287.4	g2	[31,32]
Carboxylic C	R–COOH C—O COO	1s-3p/σ*	288.0–288.7	g3	[31,32]
O-alkyl C/carbonyl	C–OH	1s-π*	289.5-290.2	g4	[31,32]
Aromatic C	C—C	1s-σ*	~291.0	g5, g6	[33-35]

Table 3: Product yield and gas composition from the pyrolysis/CVD processing of polypropylene and polystyrene.

Product yield (wt.%)	Polypropylene	Polystyrene
Gas	36.3	15.6
Oil *	27.7	51.0
Pyrolysis char	2.5	3.0
Catalyst carbon deposits	33.5	29.5
Volumetric gas concentration (vol.%)	Polypropylene	Polystyrene
CO	4.7	0.0
H_2	65.1	78.8
CO_2	0.4	2.7
CH_4	21.3	13.6
C_2-C_4	8.5	5.0

* = by difference.

Table 4. Extended X-ray Absorption Fine Structure (EXAFS) fitting for the Fe-Ni/Al_2O_3 catalyst after pyrolysis/CVD of polypropylene (PP-CNT).

Path	Coordination Number (N)	Distance R (Å)	σ^2 (Å^2) x 10^{-3}	
Fe-Fe	2.3 ± 0.3	2.46 ± 0.02	5.2 ± 1.1	
Fe-Ni	4.6 ± 0.6	2.53 ± 0.02	5.2 ± 1.1	ΔE_0 = 0.2 ± 1.3
Fe-Fe_2	1.6 ± 0.7	3.48 ± 0.02	5.2 ± 1.1	$X^2_{reduced}$= 361
Fe-Ni_2	6.9 ± 1.6	4.36 ± 0.02	5.2 ± 1.1	R-factor = 0.9%
MS (multiple scattering)	12.3 ± 3.5	5.11 ± 0.02	10.4 ± 2.2	

Table 5: Results of non-linear least squares fitting. Centroid energy, peak area (A_g) and FWHM (full-width half maxima) are given for Gaussian's g1-g6.

Gaussian functions		com-MWCNT	Polypropylene MWCNTs	Polystyrene MWCNTs
	Centroid (eV)	285.5	285.4	285.4
g1	A_g	3.56	4.24	3.48
	FWHM	1.58	1.53	1.65
	Centroid (eV)	287.2	286.9	287.1
g2	A_g	1.3	1.1	1.23
	FWHM	1.65	1.31	1.65
	Centroid (eV)	288.7	288.1	288.6
g3	A_g	1.05	1.38	1.26
	FWHM	1.61	1.54	1.65
	Centroid (eV)	289.9	289.6	290
g4	A_g	0.28	1.15	0.63
	FWHM	1.18	1.65	1.41
	Centroid (eV)	291.9	291.9	291.8
g5	A_g	1.8	3.26	1.84
	FWHM	1.36	1.53	1.23
	Centroid (eV)	293.1	293.3	293
g6	A_g	1.77	2.03	1.8
	FWHM	1.1	1.16	1.65

FIGURE CAPTIONS

Figure 1: Schematic diagram of the two-stage, pyrolysis/CVD reactor system.

Figure 2: Annotated X-ray diffraction profiles of the freshly prepared Ni-Fe/Al_2O_3 catalyst and the used Ni-Fe/Al_2O_3 catalyst used after pyrolysis/CVD of polypropylene and polystyrene.

Figure 3: (a) Fe K-edge XANES spectra of the used Ni-Fe/Al2O3 catalyst after pyrolysis/CVD of polypropylene (PP-CNT) and polystyrene PS-CNT, with the standard iron foil spectrum. (b) Magnitude of the Fourier transformed EXAFS data for PP-CNT (black circles) and the resulting EXAFS fit (solid red) for the Fe-Ni structure (inset), the EXAFS fitting range (1 – 5.5 A) is shown as vertical dotted lines.

Figure 4: (a) TGA and (b) DTG thermograms from temperature programmed oxidation of the catalyst carbon deposits from pyrolysis/CVD processing of polypropylene (PP-CNT), polystyrene (PS-CNT) and commercial MWCNTs (com-MWCNT).

Figure 5: SEM images of the freshly prepared Ni-Fe/Al_2O_3, catalyst, and the used catalysts after pyrolysis/CVD processing of the waste polypropylene and waste polystyrene. SEM magnifications are at 10,000 and 20,000 as indicated by the scale bars.

Figure 6: TEM images of the MWCNTs produced from the pyrolysis/CVD processing of waste polypropylene, waste polystyrene and commercially obtained MWCNTs (com-MWCNTs). TEM magnifications indicated by the scale bars.

Figure 7: Optical Raman spectroscopy of PS-CNT, PP-CNT and Com-MWCNT, with I_D/I_G ratios shown.

Figure 8: (a) XRS spectra for commercially obtained for MWCNTs (com-MWCNT), MWCNTs produced from pyrolysis/CVD processing of polypropylene (PP-CNT) and from polystyrene (PS-CNT) and fitted XRS spectra for (b) com-MWCNT, (c) PP-CNT and (d) PS-CNT. Gaussian centroid energies, areas and FWHM can be found in Table 4.

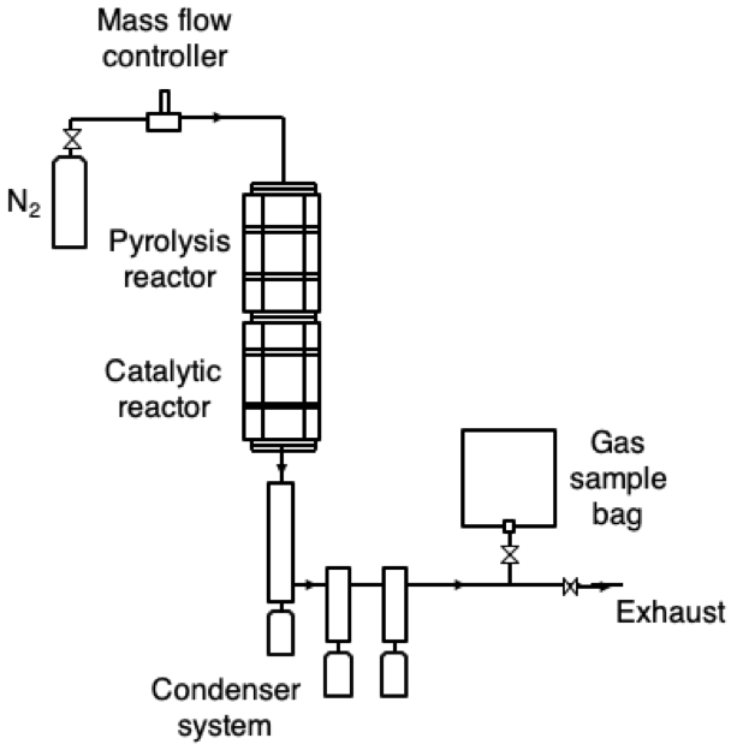

Figure 1: Schematic diagram of the two-stage, pyrolysis/CVD reactor system.

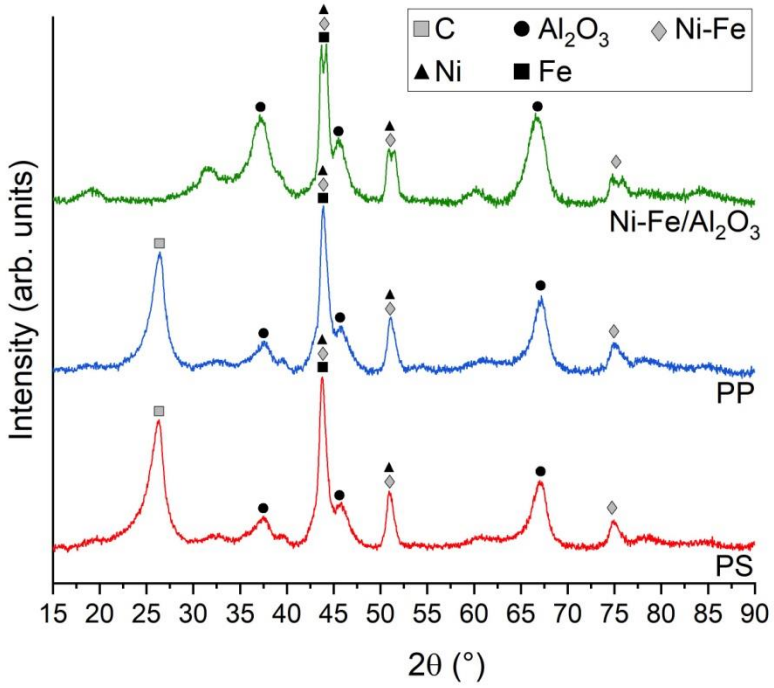

Figure 2: Annotated X-ray diffraction profiles of the freshly prepared Ni-Fe/Al_2O_3 catalyst and the used Ni-Fe/Al_2O_3 catalyst after pyrolysis/CVD of polypropylene and polystyrene.

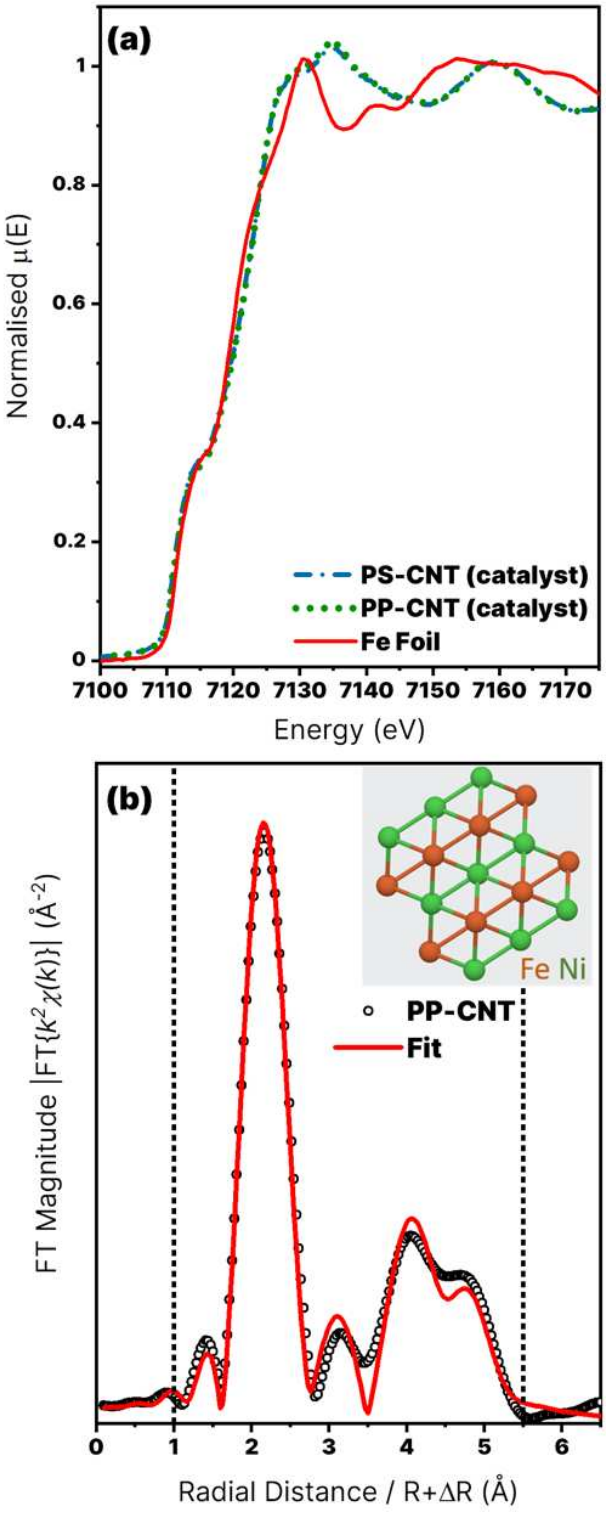

Figure 3: (a) Fe K-edge XANES spectra of the used Ni-Fe/Al2O3 catalyst after pyrolysis/CVD of polypropylene (PP-CNT) and polystyrene PS-CNT, with the standard iron foil spectrum. (b) Magnitude of the Fourier transformed EXAFS data for PP-CNT (black circles) and the resulting EXAFS fit (solid red) for the Fe-Ni structure (inset), the EXAFS fitting range (1 – 5.5 A) is shown as vertical dotted lines.

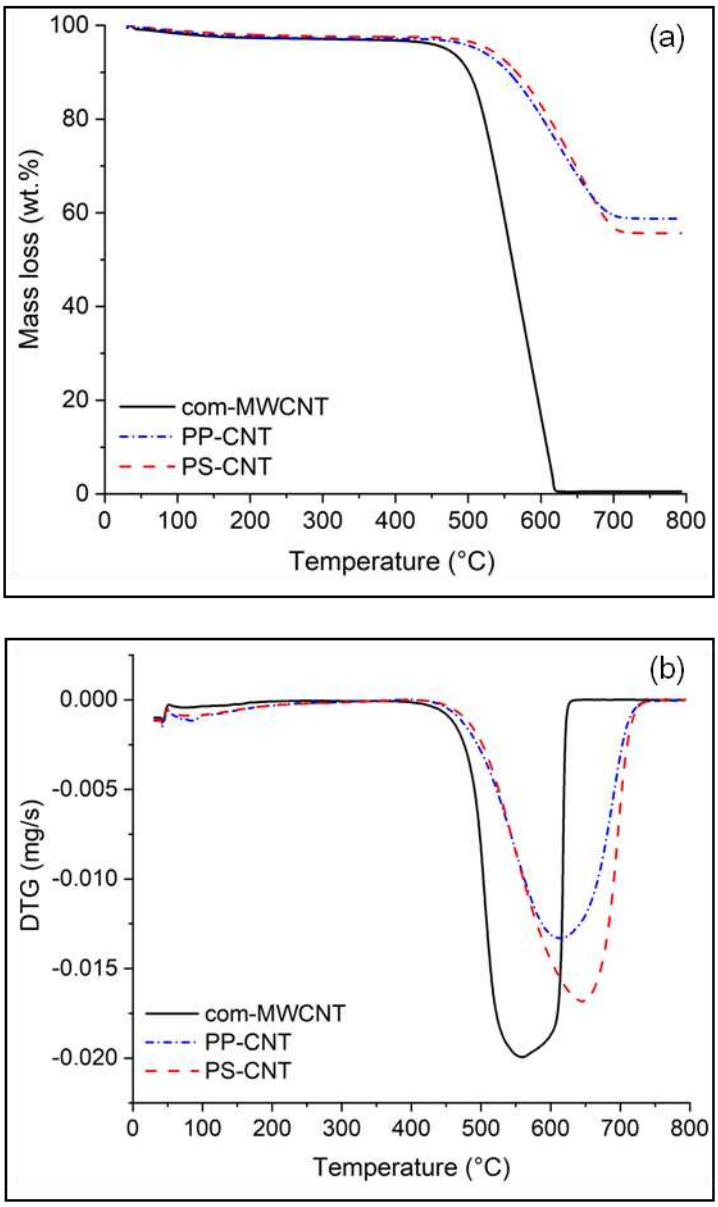

Figure 4: (a) TGA and (b) DTG thermograms from temperature programmed oxidation of the catalyst carbon deposits from pyrolysis/CVD processing of polypropylene (PP-CNT), polystyrene (PS-CNT) and commercial MWCNTs (com-MWCNT).

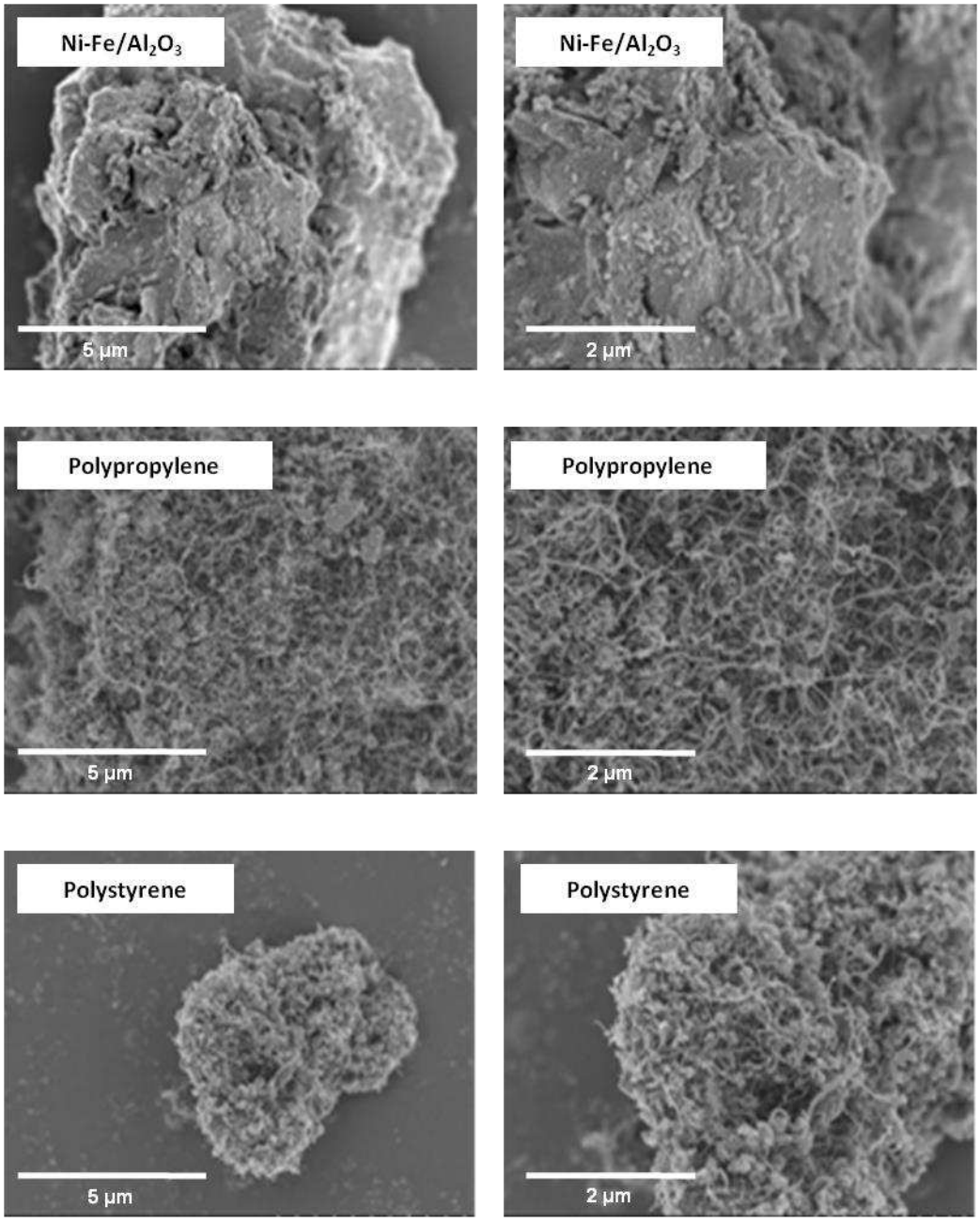

Figure 5: SEM (back-scattered electron) images of the freshly prepared Ni-Fe/Al_2O_3, catalyst, and the used catalysts after pyrolysis/CVD processing of the waste polypropylene and waste polystyrene. SEM magnifications are at 10,000 and 20,000 as indicated by the scale bars.

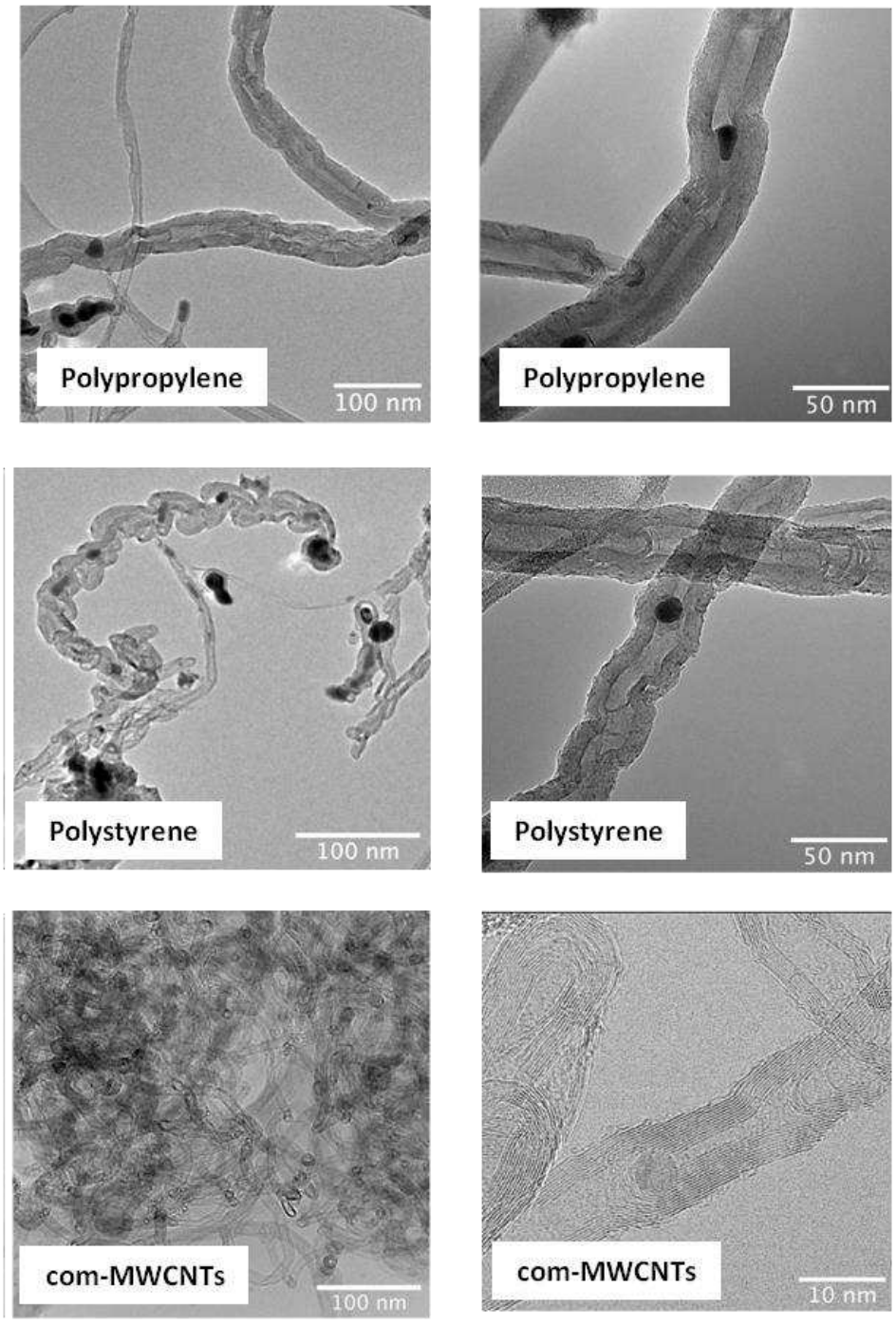

Figure 6: TEM images of the MWCNTs produced from the pyrolysis/CVD processing of waste polypropylene, waste polystyrene and com-MWCNTs.

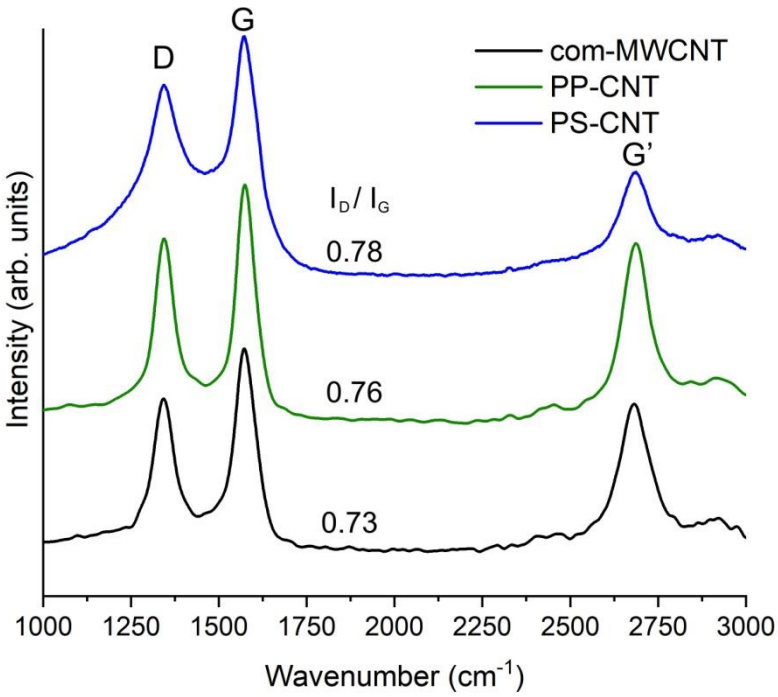

Figure 7: Optical Raman spectroscopy of PS-CNT, PP-CNT and Com-MWCNT, with I_D/I_G ratios shown.

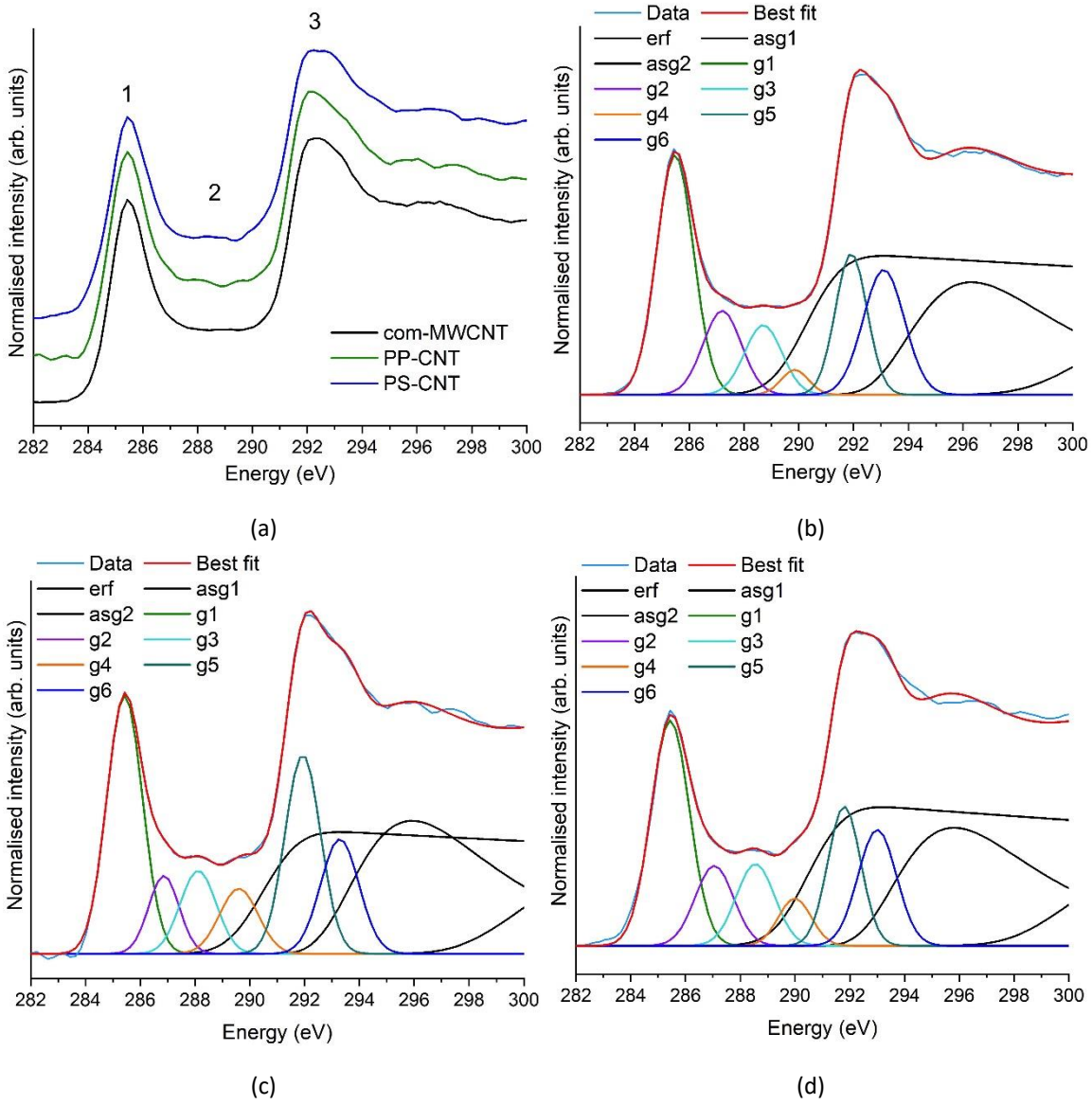

Figure 8: (a) X-ray Raman scattering spectra for commercially obtained for MWCNTs (com-MWCNT), MWCNTs produced from pyrolysis/CVD processing of polypropylene (PP-CNT) and from polystyrene (PS-CNT) and fitted XRS spectra for (b) com-MWCNT, (c) PP-CNT and (d) PS-CNT. Gaussian centroid energies, areas and FWHM can be found in Table 4.